Zirconia-Stabilized 25-Å TiO_2 Anatase Crystallites in a Mesoporous Structure

S. H. Elder,* Y. Gao, X. Li, J. Liu, D. E. McCready, and C. F. Windisch, Jr.

Departments of Materials and Chemical Sciences and Interfacial and Processing Science, Pacific Northwest National Laboratory, Richland, Washington 99352

Received April 2, 1998. Revised Manuscript Received June 11, 1998

We have prepared and characterized a mesoporous material where the framework, of both the as-synthesized and calcined materials, is composed of ZrO_2-doped 25-Å TiO_2 anatase crystallites. The nanocrystalline framework is structured about a surfactant-templated, disordered porous network with a uniform pore diameter of 28 Å. Air calcination at 450 °C removes the surfactant to yield a mesoporous solid with surface area of 330 m^2/g. The mesoporous framework and TiO_2 crystallite size are surprisingly robust, and we observed no substantial structural differences between precalcined and calcined products.

Introduction

In the field of mesoporous materials most of the published experimental research has focused on silica as the inorganic framework constituent.[1−11] In general, mesoporous silica has been prepared by the hydrolysis of tetraethyl orthosilicate in the presence of a structure-directing agent (surfactant micelles) resulting in the precipitation of mesoporous silica. The surfactant micelles are removed by thermal oxidation (calcined in air or oxygen) leaving only a porous network of amorphous silica. The pore structure is defined by the once present micelles.

The application of the reaction schemes and mechanistic models for silica have been less successful for the synthesis and understanding of mesoporous transition metal oxides. One difficulty faced with synthesizing mesoporous transition metal oxides is the thermal instability of the inorganic framework during calcination. The facile crystallization of most transition metal oxides and subsequent grain growth has been observed to result in inorganic framework rearrangements, mesopore collapse, and loss of surface area during calcination of as-synthesized mesoporous transition metal oxides.[12−17]

The goal of this work was to develop a novel synthetic approach that would permit the synthesis of thermally stable mesoporous TiO_2 either by preventing the nucleation of TiO_2 crystallites or by stabilizing nanosized TiO_2 crystallites once they formed in the framework. The synthesis and characterization of quantum-sized (1−10 nm) particles, including TiO_2, have been intensively studied in the past 10 years.[18] These studies have shown that the electronic and magnetic properties of materials can profoundly change as particle size decreases. Unfortunately, quantum-sized particles exhibit poor thermal stability due to their high surface energy. As a result, particle agglomeration and growth are difficult to prevent. Herein, we report our successful results in stabilizing TiO_2 anatase nanocrystallites in a mesoporous structure.

Experimental Section

The synthesis of the zirconia-doped mesoporous anatase TiO_2 is straightforward. In addition, all reactants are aqueous-

* To whom correspondence should be addressed.

(1) Kresge, C. T.; Leonowicz, M. E.; Roth, W. J.; Vartulli, J. C.; Beck, J. S. *Nature* **1992**, *359*, 710.
(2) Beck, J. S.; et al. *J. Am. Chem. Soc.* **1992**, *114*, 10834.
(3) Israelachvili, J. N.; Mitchell, D. J. and Ninham, B. W. *J. Chem. Soc., Faraday Trans. 2* **1976**, *72*, 1527.
(4) Raman, N. K.; Anderson, M. T.; Brinker, C. J. *Chem. Mater.* **1996**, *8*, 1682.
(5) Liu, J.; et al. *Adv. Colloid Interface Sci.* **1996**, *69*, 131.
(6) Huo, Q.; et al. *Chem. Mater.* **1994**, *6*, 1176.
(7) Firouzi, A.; et al. *Science* **1995**, *267*, 1138.
(8) Sayari, A. *Chem. Mater.* **1996**, *8*, 1840.
(9) Bagshaw, S. A.; Prouzet, E.; Pinnavaia, T. J. *Science* **1995**, *267*, 865.
(10) Prouzet, E.; Pinnavaia, T. J. *Angew. Chem., Int. Ed. Engl.* **1997**, *36*, 6 (5), 516.
(11) McGrath, K. M.; Dabbs, D. M.; Yao, N.; Aksay, I. A.; Gruner, S. M. *Science* **1997**, *277*, 552.
(12) Tian, Z.-R.; Tong, W.; Wang, J.-Y.; Duan, N.-G.; Krishnan, V.; Suib, S. L. *Science* **1997**, *276*, 926.
(13) (a) Antonelli, D. M.; Ying, J. Y. *Angew. Chem., Int. Ed. Engl.* **1995**, *34*, 4 (18), 2014. (b) Putnam, R. L.; Nakagawa, N.; McGrath, K. M.; Yao, N.; Aksay, I. A.; Gruner, S. M.; Navrotsky, A. *Chem. Mater.* **1997**, *9*, 2690.
(14) Kim, A.; Bruinsma, P.; Chen, Y.; Wang, L.-Q.; Liu, J. *Chem. Commun.* **1997**, 161.
(15) Ulagappan, N.; Rao, C. N. R. *Chem. Commun.* **1996**, 1685.
(16) Antonelli, D. M. and Ying, J. Y. *Angew. Chem., Int. Ed. Engl.* **1996**, *35*, 426.
(17) Antonelli, D. M.; Ying, J. Y. *Chem. Mater.* **1996**, *8*, 874.
(18) Liu, Y. and Claus, R. O. *J. Am. Chem. Soc.* **1997**, *119*, 5273. (b) Liu, Y.; Wang, A.; Claus, R. O. *J. Phys. Chem. B* **1997**, *101*, 1385. (c) Choi, W.; Termin, A.; Hoffmann, M. R. *J. Phys. Chem.* **1994**, *98*, 13669. (d) Joselevich, E.; Willner, I. *J. Phys. Chem.* **1994**, *98*, 7628. (e) Haase, M.; Weller, H.; Henglein, A. *J. Phys. Chem.* **1988**, *92*, 4706. (f) Rossetti, R.; Ellison, J. L.; Gibson, J. M.; Brus, L. E. *J. Phys. Chem.* **1984**, *80*, 4403. (g) Bahnemann, D. W. *Isr. J. Chem.* **1993**, *33*, 115. (h) Graetzel, M. *Chemistry and Physics of Solid Surfaces V*; Howe, R., Vanselow, R., Eds.; Springer-Verlag: Berlin, New York; 1984. (i) Henglein, I. *Top. Curr. Chem.* **1988**, *143*, 113. (j) Henglein, A. *Chem. Rev.* **1989**, *89*, 1861. (k) Wang, Y. *Acc. Chem. Res.* **1991**, *24*, 133. (l) Brus, L. E. *J. Phys. Chem.* **1986**, *90*, 2555. (m) Steigerwald, M. L.; Brus, L. E. *Acc. Chem. Res.* **1990**, *23*, 183. (n) Lippens, P. E.; Lannoo, M. *Phys. Rev. B* **1989**, *39*, 10935. (o) Tran, Thoai, D. B.; Hu, Y. Z.; Koch, S. W. *Phys. Rev. B* **1990**, *42*, 11261. (p) Henglein, A. *Isr. J. Chem.* **1993**, *33*, 115. (q) Moser, J.; Gratzel, M.; Gallay, R. *Helv. Chim. Acta* **1987**, *70*, 1596.

10.1021/cm980237i CCC: $15.00
Published on Web 08/22/1998

based, inexpensive, readily available on a large scale, and environmentally friendly. $(NH_4)_2Ti(OH)_2(C_3H_5O_3)_2$ (Tyzor LA—from DuPont, 2.23M in Ti), $(NH_4)_2Zr(OH)_2(CO_3)_2$ (AZC—from Magnesium Electron Inc., 14.8 wt % Zr), and cetyltrimethylammonium chloride (CTAC, 29 wt %, from Lonza Chemical Co., Inc.) are combined in a 3 Ti:1 Zr:2 CTAC molar ratio. The resulting clear mixture is stirred while slowly adding water. A white precipitate immediately forms but readily dissolves upon stirring. Precipitate formation and dissolution continue until the original mixture is diluted by a factor of ~5, at which point irreversible precipitation occurs. Irreversible precipitation continues until the original mixture is diluted by a factor of 10. The sticky, white precipitate is stirred overnight at room temperature (UNAGED PPT) and aged for 60 h at 100 °C and overnight at 150 °C in a sealed Teflon reactor (AGED PPT). The AGED PPT is isolated by washing and centrifuging several times with fresh aliquots of water and drying at 40 °C for at least 24 h. AGED PPT is heated in air at 160 °C/h to 450 °C where it is calcined for 2 h. The resultant solid is a free-flowing, white powder (PNNL-1). Elemental analysis on PNNL-1 confirmed the 3:1 Ti:Zr ratio.

Two control syntheses were performed in a similar fashion as for PNNL-1 except in the first case no CTAC was used (no. 1), and in the second case NH_4Cl was substituted for CTAC (no. 2). No precipitation occurred at room temperature in either case, but after hydrothermal aging a translucent physical gel was produced in each control.

X-ray powder diffraction (XRPD) data were obtained with a Philips X′PERT-MPD diffractometer using Cu Kα radiation. Transmission electron microscopy (TEM) data were obtained on a JEOL JEM−2010-electron microscope. The UNAGED PPT TEM sample was prepared by placing a drop from the aqueous reaction mixture directly on a holey carbon coated Cu grid. AGED PPT and PNNL-1 TEM samples were prepared by first suspending the powders in ethanol and placing a drop of the solution on a holey carbon coated Cu grid. Nitrogen adsorption/desorption measurements were collected with the Quantachrome Autosorb 6-B gas sorption system on degassed samples at 77 K. Raman spectra were collected with a Spex Industries model 1877 triple raman spectrometer (Edison, NJ) with the 488.0 nm line of a Spectra Physics model 164 argon ion laser (Mountain View, CA) for excitation and a Princeton Instruments LN/CCD detector (Trenton, NJ). Typically, spectra were obtained on the liquid samples by using a 90° scattering configuration and a single exposure of 100 s. The slit width was 400 μm. Spectral analysis was performed by using Galactic Industries Grams/368 software (Salem, NH). The estimated uncertainty of the peak frequencies was ±2 cm^{-1}.

Results and Discussion

The stability and reactivity of a Tyzor LA/AZC/CTAC mixture is markedly influenced by the addition of water—on dilution a rapid reaction between the inorganic precursors and CTAC occurs which results in a precipitate with a surfactant filled porous network. In contrast, no precipitation occurs in similar reactions if CTAC is absent (control 1) or if CTAC is replaced by NH_4Cl (control 2). The experimental data that follow are consistent with CTAC not only influencing the stability of the inorganic precursors, but also the structural characteristics of the hydrthermally aged and calcined precipitate.

TEM images of UNAGED PPT, AGED PPT, and PNNL-1 are shown in Figure 1a−c. These figures show a relatively large area and reveal a porous structure where surfactant-filled pores (Figure 1a,b) appear white and the TiO_2/ZrO_2 framework is dark. TEM images of these samples, taken at low magnification (<200000X), show very low contrast due to the small particle and pore sizes (~25 Å). Unlike mesoporous silica where the thickness changes abruptly between silica wall edge and the pore, the thickness of the nanosized TiO_2/ZrO_2 particles decreases continuously from the center to the edge. The result is weak diffraction contrast even at large underfocus conditions. Slight differences in image contrast are visible for these samples. The additional dark areas in PNNL-1 are actually due to the overlapping of nanosized particles with pores, not decreased porosity. Figure 1a−c exhibits a nearly monodispersed pore size with a mean diameter of ~30 Å. For comparison, TEM images of the gels from controls 1 and 2 revealed an open network of randomly interconnected particles (>50 Å in diameter) with large, irregularly shaped pores ranging in size from 75 to 150 Å. This suggests the regular porous structure of UNAGED PPT and AGED PPT is caused by CTAC. In addition, the high-resolution TEM (HRTEM) image of AGED PPT (Figure 1d) exhibits anatase lattice fringes in many of the particles, indicating that these crystallites are formed in the aqueous solution. Similar lattice fringes were observed in the HRTEM images of UNAGED PPT and PNNL-1. The pore size and structure are very similar for all three solids. Therefore, since the pore structure is filled with CTAC in UNAGED PPT and AGED PPT, it is logical to conclude the pore structure in PNNL-1 is a direct result of the CTAC shape and continuity prior to calcination. However, Figure 1c does show two structural changes in the PNNL-1 sample as compared to UNAGED PPT and AGED PPT. First, the TiO_2 lattice quality (or crystallinity) has deteriorated, which we attribute to a ZrO_2 doping induced distortion of the TiO_2 lattice.[19,20] Second, the contrast between individual crystallites has decreased due to the increased connectivity of particles comprising the framework. These results indicate that some intermixing between TiO_2 and ZrO_2 occurred during calcination. This intermixing reduces the discretelike characteristic of the particles and leads to a more continuous-like framework. However, it has no apparent effect on the pore and particle size. This is consistent with the nitrogen adsorption/desorption data collected on PNNL-1 (vide infra). Figure 2 is an *idealized* representation of the TEM images for UNAGED PPT, AGED PPT, and PNNL-1 to highlight the most important nanoscopic structural features of these materials.

X-ray energy dispersive spectroscopy (XEDS) data from UNAGED PPT, using a 25-nm beam size, showed a large variation in the Ti/Zr ratio from Ti-rich to Zr-rich. However, XEDS analysis taken from large areas (0.5 μm diameter) yielded a Ti/Zr ratio close to the nominal 3:1 ratio, suggesting the average composition of UNAGED PPT is similar to that of the reactant stoichiometry. In comparison, XEDS on AGED PPT and PNNL-1 revealed a 3:1 Ti/Zr ratio throughout the samples by using either spot or large area analysis, pointing out that the composition became homogeneous after aging and remained homogeneous after calcining. The compositional change from heterogeneous to homogeneous during aging is in agreement with the occurrence of structural and compositional reorganization during the aging steps. Likewise, no phase separa-

(19) Gao, Y.; Liang, Y.; Chambers, S. A. *Surf. Sci.* **1996**, *348*, 17.
(20) Xu, Q.; Anderson, M. A. *J. Am. Ceram. Soc.* **1993**, *76* (8), 2093.

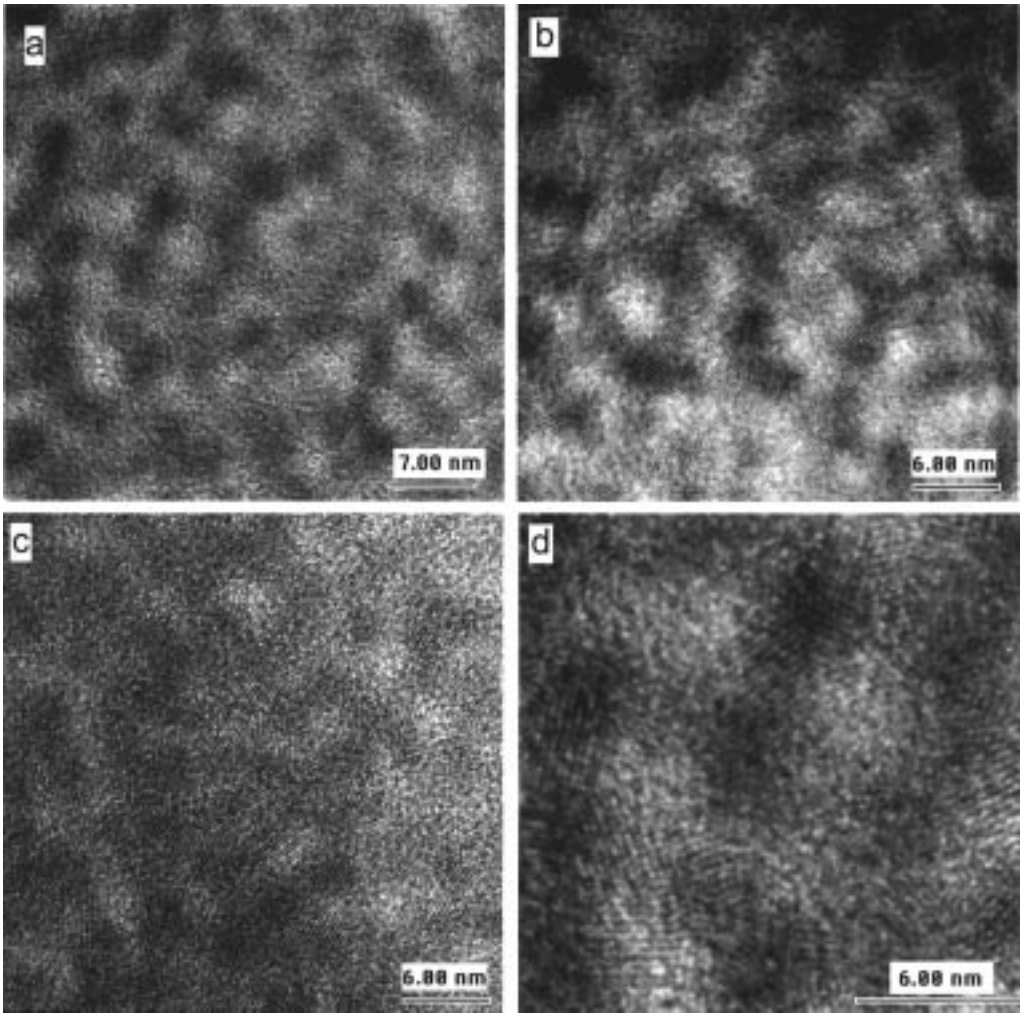

Figure 1. (a, b, c) Low magnification transmission electron micrograph of UNAGED PPT, AGED PPT, and PNNL-1; (d) high-resolution transmission electron micrograph of AGED PPT. All images indicate a narrow pore and particle size distribution, with an average size of ~30 Å each.

tion occurred during the high-temperature treatment. Instead, the formation of a $Zr_xTi_{1-x}O_2$ solid solution produced a highly distorted lattice structure at the titania/zirconia interface and thus reduced the quality of PNNL-1 anatase crystallites. In addition, XEDS data showed AGED PPT to be free of chloride.

We have not observed anatase crystallites significantly larger than 30 Å in our TEM experiments. Furthermore, these experiments have not shown PNNL-1 to contain dense (i.e., nonporous) secondary phases. These results support the model of CTAC micelles templating the mesoporous network in PNNL-1.

Figure 3 represents the XRPD data collected on AGED PPT and PNNL-1. It is clear that anatase TiO_2 is present in both materials (peaks marked with a). PNNL-1 also has a broad peak (marked with b) centered at ~30°, which is in agreement with amorphous material in the framework. The partial amorphization is consistent with the TEM observation of lattice distortion in the TiO_2 crystallites (Figure 1c). We are uncertain of the structural feature in AGED PPT that leads to the very broad peak observed at ~20° (marked with c). The average anatase crystallite size is 30 Å, based upon Scherrer line broadening.[21] Both XRPD patterns in Figure 3 exhibit single, well-defined low angle peaks (~1.8°) centered at $d \sim 50$ Å, which is expected for the pore center-to-pore center dimension of the poorly ordered mesoporous structure observed in Figures 1b,c (sum of the wall thickness 25−30 Å from TEM and XRPD and pore diameter 25−30 Å from TEM and N_2 adsorption experiments).[22] The intensity of the low angle peak for AGED PPT is about twice that of PNNL-1 due to slight variations in sample mounting which can significantly influence the low angle XRPD data. Therefore, the intensities of all the AGED PPT reflections in Figure 3 were doubled so the reflections due to anatase could be relatively compared. The lack of higher order (*hkl*) reflections associated with the low angle peaks again supports a mesoporous structure that lacks order.[9−11,22]

Figure 4A depicts the N_2 adsorption/desorption isotherm for PNNL-1, Figure 4B the Barrett−Joyner−Halenda (BJH) cumulative adsorption pore volume (BJH−CAPV), and Figure 4C the BJH pore size distribution for the adsorption data.[23] The slope in the isotherm curve between P/P_o of 0.1−0.4 is in accord with

(21) Cullity, B. D. *Elements of X-ray Diffraction*, ed. 2; Addison-Wesley Publishing Co.; Reading, MA, 1978; p 284.
(22) Guinier, A.; Fournet, G. *Small-Angle Scattering of X-rays*; John Wiley & Sons: New York, 1955; pp 203−208.
(23) Barrett, E. P.; Joyner, L. G.; Halenda, P. P. *J. Am. Chem. Soc.* **1951**, *73*, 373.

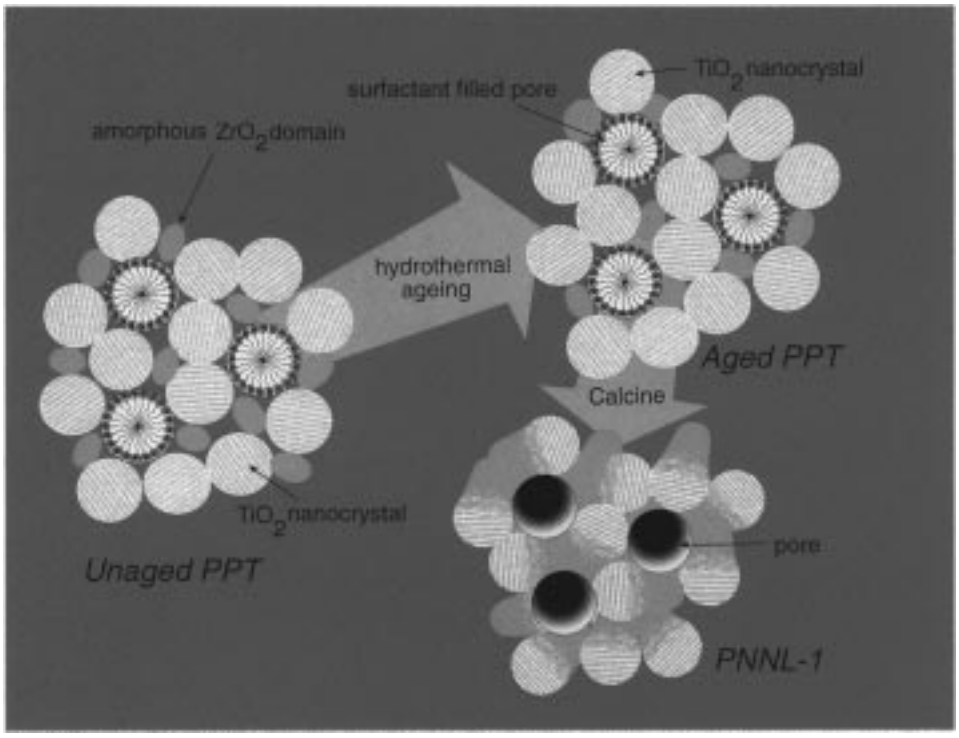

Figure 2. *Idealized* schematic representations of UNAGED PPT, AGED PPT, and PNNL-1 showing the perpendicular cross section of three pores and the inorganic framework structured about those pores. The structural arrangements of UNAGED PPT and AGED PPT are rather similar except there is an increased degree of framework condensation in AGED PPT due to the elimination of coordinated lactate (not shown for clarity). The undulating lines in the TiO_2 nanocrystals of PNNL-1 represent amorphization of the lattice due to Zr doping.

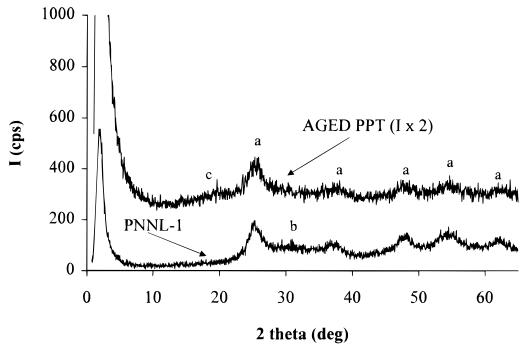

Figure 3. X-ray powder diffraction (XRPD) patterns for AGED PPT and PNNL-1. The low angle peaks (~1.8°) in both patterns correspond to the pore center-to-center dimension in the mesoporous network. The peaks marked (a) are indexed as anatase TiO_2, (b) a broad peak due to amorphous material, and we are uncertain of the origin of the peak marked (c).

enhanced or cooperative N_2 adsorption.[24] This effect can be especially pronounced in pores with diameters <30 Å due to the pores being only a few adsorbate molecules wide (~6 N_2 molecules in this case). The enhanced adsorption in this relative pressure range is not uncommon for type IV isotherms (for small mesopore materials with pore diameters in the 20−30 Å range) and is a consequence of lateral interactions between pore wall surfaces and nonsurface adsorbate molecules.[24] In addition, this general isotherm shape has been observed in mesoporous silica, alumina, and zirconia systems and was attributed to the poorly ordered nature of the mesoporous network and small mesopores.[10,25−27] In the case of PNNL-1, framework texturing due to the presence of nanocrystallites may also lead to small variations in pore diameter. The Brunauer−Emmett−Teller (BET) specific surface area, calculated from the isotherm data in the relative pressure range 0.1−0.3, is 330 m^2/g.[28] For comparison, using the modified BJH method, a surface area of 300 m^2/g was calculated for pores with diameter of 20−40 Å.[29] As previously discussed, based on both the TEM and XRPD data (Figures 1 and 3), the average pore diameter is expected to be 25−30 Å. It has been noted that the Kelvin equation may not be strictly valid for pore diameters less than ~35 Å due to possible instabilities of the adsorbate meniscus.[24] This does introduce some limitations when interpreting BJH pore size distribution data since it is based in part on the Kelvin equation. However, recent work illustrates the utility of the Kelvin equation and the BJH formalism for pore analysis of MCM-41 materials with diameters in the range of 28−66 Å.[29] Taking this into consideration, the BJH−CAPV shown in Figure 4B distinctly shows the majority of the nitrogen uptake occurs in the pore diameter range 20−40 Å. The average BJH pore size from Figure 4C is 28 Å, which is similar to what has been reported for CTAC templated pores in mesoporous silica materials. The pore size distribution at full width, half-maximum is ~15 Å. Nitrogen adsorption experiments indicated the calcined

(24) Gregg, S. J.; Sing, K. S. W. *Adsorption, Surface Area and Porosity*, 2nd ed.; Academic Press: San Diego, 1982.
(25) Sayari, A.; Liu, P.; Kruk, M.; Jaroniec, M. *Chem. Mater.*, in press.
(26) Vaudry, F.; Khodabandeh, S.; Davis, M. E. *Chem. Mater.* **1996**, *8*, 1451.
(27) Ciesla, U.; Schacht, S.; Stucky, G. D.; Unger, K. K.; Schuth, F. *Angew. Chem., Int. Ed. Engl.* **1996**, *35* (5), 541.
(28) Brunauer, S.; Emmett, P. H.; Teller, E. *J. Am. Chem. Soc.* **1938**, *60*, 309.
(29) Kruk, M.; Jaroniec, M.; Sayari, A. *Langmuir* **1997**, *13*, 6267.

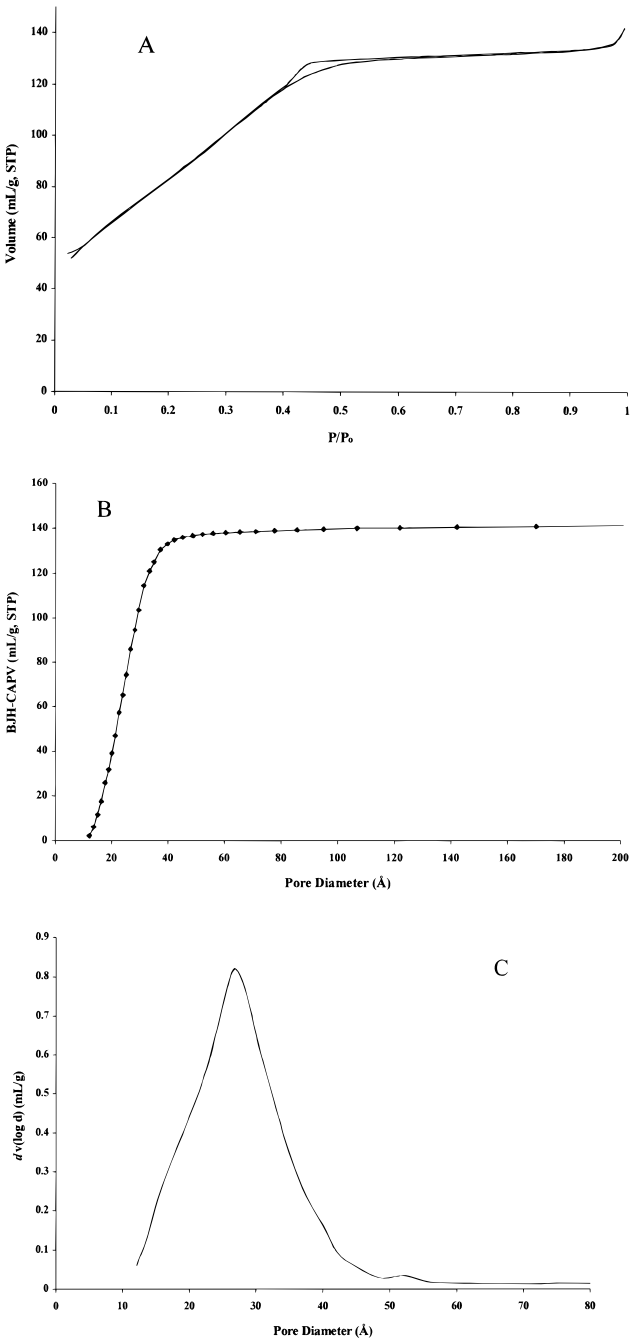

Figure 4. (A) N_2 adsorption/desorption isotherm for PNNL-1; P/P_0 is the partial pressure of N_2 in equilibrium with the sample at 77 K. (B) BJH cumulative adsorption pore volume (BJH−CAPV) for PNNL-1. (C) BJH pore size distribution calculated from the PNNL-1 adsorption isotherm data.

gels from controls 1 and 2 were microporous with BET specific surface areas of around 220 m^2/g. Moreover, BJH pore size data showed *no* indication of narrow pore size distributions.

We believe the unique chemical and structural characteristics of Tyzor LA, along with the ZrO_2 doping, are the primary reasons we have been successful in preparing stable 25 Å TiO_2 crystallites in the framework of PNNL-1. Recent studies have indicated the discrete molecular unit depicted in the Tyzor LA chemical formula does not represent the equilibrium solution species.[30,31] Instead, NMR and Raman scattering data suggest the molecular units condense forming *anionic* clusters consisting of an anatase-like interior with lactate coordinating the outside. They estimated the clusters to contain 12 titanium atoms.[31] It is these lactate-stabilized TiO_2 nanoclusters that rapidly condense to assemble the remarkably narrow size range of anatase nanocrystallites (Figure 1b) during the formation of AGED PPT.

Considering these structural results on Tyzor LA and our synthetic results, we propose the inorganic precursor/CTAC reaction mechanism for the formation of UNAGED PPT and AGED PPT is akin to that proposed by Monnier and co-workers,[32] with the exception that long-range micellar ordering does not occur. The addition of water to a Tyzor LA/AZC mixture produces *no* precipitate at room temperature. However, the presence of CTAC, combined with a change in concentration with addition of water, does significantly alter the chemical and electrostatic interactions between inorganic polyanions. The first drop of water added to the Tyzor LA/AZC/CTAC solution results in a precipitate, but it redissolves on stirring. In the diluted region where precipitation occurs, the inorganic−surfactant Coulombic interactions change, permitting inorganic polyanions to partially condense. We have found the 150 °C hydrothermal aging imperative to fully condense the framework and give thermal stability during calcination. HRTEM images of dried Tyzor LA (no CTAC present) do not show the presence of TiO_2 nanocrystallites or regular porosity. This strongly indicates the particle and pore arrangement in the framework of AGED PPT and PNNL-1 (Figure 1b,c) is not due to simple random particle packing, but instead the micelle surfaces provide nucleation sites and structural templates for Tyzor LA/AZC condensation. Gravimetric data collected on AGED PPT confirmed the presence of five surfactant molecules per metal atom.

In support of this condensation mechanism, we collected Raman scattering data on a series of Tyzor LA solutions diluted with water. These experiments monitored the relative amounts of lactate coordinated to Ti versus free lactate in solution. The coordinated lactate-to-free lactate ratio (C/F) is approximately 1 in the stock Tyzor LA solution. The C/F ratio remains constant until the stock Tyzor LA solution has been diluted with water by a factor of about 11. At dilution rates greater than 11, C/F dramatically drops to ~0.4, signaling a loss of coordinated lactate. However, no precipitation due to cluster condensation occurs, because the solution is quite dilute. Similar Raman scattering behavior was observed for a Tyzor LA/CTAC dilution series, but the dramatic C/F drop occurred at a dilution of approximately seven. This is near the point of dilution where irreversible precipitation is observed in the synthesis of UNAGED PPT. These experiments also confirmed the presence of lactate coordinated to titanium in UNAGED PPT, but coordinated lactate is absent in AGED PPT. This indicates that hydrothermal aging of UNAGED PPT promotes ligand elimination and condensation between inorganic units. This framework condensation is likely a key factor in providing thermal stability during conversion of AGED PPT to PPNL-1.

(30) Baskaran, S.; Song, L.; Liu, J.; Chen, Y. L.; Graff, G. L. *J. Am. Ceram. Soc.*, in press.
(31) Graff, G. L.; et al., submitted to *J. Theo. Chem.*
(32) Monnier, A.; et al. *Science* **1993**, *261*, 1299. .

The preparation of mesoporous (lamellar) TiO_2 has been reported, but the material contained a significant level of phosphate as a residue from the surfactant.[13] In other words, the inorganic framework of this material contained Ti, O, and P in an amorphous arrangement. Apparently, the phosphorus substitution was necessary to form this material. Phosphorus and sulfur doping stabilization of mesoporous ZrO_2 has also been noted.[27] The reaction mechanism for the preparation of the mesoporous ZrO_2 of Hudson and Knowles' was determined not to be a cooperative electrostatic and chemically induced interaction between micelles and inorganic anions.[33] They concluded the surfactant micelles simply acted as a *scaffolding shape* about which zirconia gelation occurred. In comparison, the precipitation of UNAGED PPT is clearly a result of a cooperative interaction between surfactant micelles and inorganic polyanions.

The framework structure of AGED PPT and PNNL-1 is strikingly different than in the aforementioned TiO_2 and ZrO_2 materials. In those examples the inorganic framework is amorphous. The feature most unusual about UNAGED PPT, AGED PPT, and PNNL-1 is the presence of 25-Å TiO_2 anatase crystallites that *do not* significantly change in size during hydrothermal and calcining treatment. We believe these to be the smallest, thermally stable crystallites of TiO_2 ever reported.[18] There is good agreement between the HRTEM images (Figure 1), the XRPD data (Figure 3), and the nitrogen adsorption/desorption data (Figure 4) concerning the structural features of these three materials. The data convincingly point to a structure containing a poorly ordered porous network with average pore diameter of 28 Å. The framework of UNAGED PPT and AGED PPT are quite similar and consist of ~25-Å TiO_2 anatase crystallites with interspersed amorphous zirconia regions. The framework of PNNL-1 differs from UNAGED PPT and AGED PPT only in that the TiO_2 crystallite quality has decreased due to Zr substitution on Ti sites in the anatase structure. We believe the Zr doping is the key factor for the framework stability of PNNL-1. The Zr substitution causes partial amorphization of the anatase lattice (see Figure 1c) through strain distortion. The substitution-induced strain arises from the size disparity between Zr^{4+} (r = 0.72 Å) and Ti^{4+} (r = 0.61 Å).[19] The HRTEM images show zirconia may also reside between the TiO_2 crystallites, effectively producing a diffusion barrier to TiO_2 particle growth.[20] The low temperature and short calcination time prevent the formation of the thermodynamic equilibrium $ZrTiO_4$ phase, which is consistent with the report of Xu and Anderson.[20]

In summary, the capacity to synthesize mesoporous *crystalline* transition metal materials is of great significance because specific crystallographic and electronic structures of solid state compounds are required in certain technological applications. For example, anatase appears to be the most photocatalytically and electrochemically active crystallographic form of TiO_2, as opposed to the rutile and brookite forms.[34,35] Furthermore, the stabilization of *nanoparticle* TiO_2 in PNNL-1 may have far-reaching implications for its use as a photocatalytic material. The unique structural and chemical characteristics of Tyzor LA provide a pathway to prepare surfactant directed mesoporous TiO_2 where the crystalline structure of the inorganic framework is a direct result of the metal precursor structure. As a consequence, we are considering similar precursors and reaction schemes for the synthesis of other crystalline mesoporous transition metal materials not yet realized through conventional routes.

Acknowledgment. This work was performed at Pacific Northwest National Laboratory, a multiprogram laboratory operated by Battelle for the U. S. Department of Energy. S.H.E. thanks Dr. Martin Thomas and Prof. Mietek Jaroniec for insightful discussions concerning the N_2 adsorption data. The authors gratefully acknowledge the Office of Basic Energy Sciences, Division of Materials Science, Project #26100, for supporting this work.

CM980237I

(33) Hudson, M. J.; Knowles, J. A. *J. Mater. Chem.* **1996**, *6* (1), 89.

(34) Hoffmann, M. R.; Martin, S. T.; Choi, W.; Bahnemann, D. W. *Chem. Rev.* **1995**, *95*, 69.

(35) Huang, S. Y.; Kavan, L.; Exnar, I.; Gratzel,M. *J. Electrochem. Soc.* **1995**, *9*, L142.